Scattering by inductive post in uniformly curved rectangular waveguide

Igor V. Petrusenko[1] and Vitaliy P. Chumachenko[2]

[1]Electronics Engineering Department, Gebze Institute of Technology, Gebze, Kocaeli 41400, Turkey

[2]Zaporizhzhia National Technical University, 64 Zhukovsky Str., Zaporizhzhia, 69063 Ukraine

Abstract. *The rigorous solution to the problem of wave scattering by a single inductive post in a continuously curved rectangular waveguide is presented. The position of the post and its radius are arbitrary. The waveguide curvature can be varied over wide limits. An efficient mathematical model of the unit is based on the domain-product technique. The theory developed is applied to the normalised reactances of the discontinuity and the induced surface current. The results obtained lend support to the validity of the known approximate solution for a thin post as far as this approximation goes. It is found that data for a centrally placed post deviate slightly from those for a straight guide in a broad interval of curvature variation. The off-centre shift affects the characteristics appreciably. Over full waveguide bandwidth, the paper provides one with the data that are essential in the design of devices containing the uniform bends, such as band-pass filters or transmission resonators, etc.*

Key words: Curved waveguide, inductive post, domain-product technique

1. Introduction

The analysis of wave scattering by inductive obstacles in a waveguide has traditionally attracted considerable attention in microwave theory [1-12]. A cylindrical post is a subject of constant interest in the design of manifold filters [1, 2, 4-12] and many other microwave devices [1-3]. Therefore, the correct analysis of the inductive posts in various waveguiding structures is of great practical importance.

The circular post in a straight rectangular waveguide has been studied in details [4-11]. The configuration has been analysed by a variety of methods. Some of them are finite- and boundary-element methods [4, 5], the technique of equivalent sources [6, 7], the variational approach [8], the Rayleigh hypothesis [9], singular integral equation method [10], domain-product technique [11].

Scattering properties of the post in a curved guide are known less, though the problem is valuable for applications as well. For example, the transmission resonators and band-pass filters containing sections with the inductive posts of both the straight rectangular waveguide and the continuously curved one can be proposed. Such filters offer certain advantages in the wave band away from the central frequency [12].

The cylindrical post in the curved waveguide is difficult to analyse using traditional techniques in view of the complicated geometry of the problem. Owing to the presence of convex and concave boundaries simultaneously, the use of full numerical techniques is not very efficient with respect to computational effort and accuracy.

This paper presents a novel rigorous solution to the problem of a circular post in a uniformly curved rectangular waveguide. The domain-product technique (DPT) [13] is applied to calculate the normalised reactances of the discontinuity and the induced surface current in a wide range of curvature variation, any possible radius and arbitrary location of the post in the interior of the waveguide bend. This approach is highly efficient compared to full numerical methods because DPT reduces the problem to the equation of the Fredholm type with nuclear matrix operator. That ensures the correct and accurate mathematical model, the absence of spurious solutions, the validity of the truncation procedure, the fast convergence of computed solution to the exact one and robust calculations.

Here we deal only with a single inductive perfectly conducting (PEC) cylinder, but the approach can be easily extended on the penetrable post with typical losses or post array placed parallel to the narrow or broad wall of the guide.

2. Problem specification and mathematical modelling

The configuration of interest and the co-ordinate systems used are shown in Fig. 1. We consider a circular post of a radius r, placed across the guide parallel to the narrow PEC wall and centered at $\rho = R_p = R_1 + d$ in the uniformly curved waveguide of the width $2a = R_2 - R_1$. The geometry is a two-dimensional one and only the electric field has nonvanishing E_y-component. The guide is filled with a homogeneous lossless medium and terminated in matching loads. The wave incident upon the post is the dominant LM_{10} mode travelling in the positive θ-direction. The convention of time dependence is $\exp(j\omega t)$ and $k = 2\pi/\lambda$ is the wavenumber.

Let us divide the interior of the bend into the regular waveguide regions I and III, and the interaction region II (Fig. 1). In regions I and III, the field can be represented in terms of LM_{m0}–mode series expansions

$$E_y^{(1)} = \psi_1(k\rho)e^{-j\nu_1(\theta+\alpha)} + \sum_{m=1}^{\infty} C_m^R \psi_m(k\rho) e^{j\nu_m(\theta+\alpha)} \tag{1}$$

$$E_y^{(3)} = \sum_{m=1}^{\infty} C_m^T \psi_m(k\rho) e^{-j\nu_m(\theta-\alpha)} \tag{2}$$

with the reflection C_m^R and transmission C_m^T coefficients to be found. The radial distributions of the modes are defined by the cross eigenfunctions

$$\psi_m(k\rho) = P_{\nu_m}(k\rho, kR_2)\left\|P_{\nu_m}\right\|^{-1}, \; m = 1, 2, ... \tag{3}$$

where

$$P_\nu(k\rho, kR_2) = J_\nu(k\rho) N_\nu(kR_2) - J_\nu(kR_2) N_\nu(k\rho) \tag{4}$$

is the cross-product Bessel function with norm $\|P_\nu\|$, J_ν and N_ν are respectively the Bessel and Neumann functions. The needed properties of $\psi_m(k\rho)$ are described in Appendix A.

The symmetry of the geometry makes it possible to subdivide the initial problem into two subproblems corresponding to the symmetric and antisymmetric excitations, subsequently referred to as “s” and “a”. Henceforth, the both types of the excitation are presented simultaneously.

According with DPT, let us imagine the interaction region II as the common part of five domains, namely

- the semi-infinite sector $\{(\rho, \theta) : \rho > R_1, -\alpha < \theta < \alpha\}$;
- the first guide $\{(\rho, \theta) : R_1 < \rho < R_2, \theta < \alpha\}$;
- the sector of annulus $\{(\rho, \theta) : \tilde{R} < \rho < R_2, -\alpha < \theta < \alpha\}$, where the value of radius $\tilde{R} \in (0, R_1)$ is virtually of no importance;
- the second guide $\{(\rho, \theta) : R_1 < \rho < R_2, \theta > -\alpha\}$;
- the exterior to the post $\{(\rho', \theta') : \rho' > r, -\pi < \theta' \le \pi\}$.

The angle $\alpha < \pi$ is assumed arbitrary, but greater than the viewing angle of the post.

Because of the linearity of the Helmholtz equation, its solution $E_y^{(2)}$ can be represented in the form

$$E_y^{(2)} = \sum_{i=1}^{5} u_i \tag{5}$$

where all the functions satisfy the same equation. Separating variables, we obtain

$$u_1 = \sum_{n=0}^{\infty} b_n^{(1)} \varphi_n(\theta) \hat{H}_n(k\rho) \tag{6}$$

$$u_3 = \sum_{n=0}^{\infty} b_n^{(3)} \varphi_n(\theta) \hat{W}_n(k\rho) \tag{7}$$

$$\varphi_n(\theta) = \cos \mu_n(\theta+\alpha), \quad \hat{H}_n = \frac{H_{\mu_n}^{(2)}(k\rho)}{H_{\mu_n}^{(2)}(kR_1)}, \quad \mu_n = \frac{n\pi}{2\alpha}$$

under qualification $\partial u_1 / \partial\theta = \partial u_3 / \partial\theta = 0$ at $\theta = \pm\alpha$ and also ${}^{\mathrm{s}}b_{2n-1}^{(1)} = {}^{\mathrm{s}}b_{2n-1}^{(3)} = 0$, ${}^{\mathrm{a}}b_{2n}^{(1)} = {}^{\mathrm{a}}b_{2n}^{(3)} = 0$. Here $H_{\mu}^{(2)}$ is symbolises the Hankel function. In (7), $\hat{W}_n$ may be any function, which is a regular solution of the Bessel equation in the interval $\tilde{R} \le \rho \le R_2$. One appropriate choice of this function is described in Appendix B.

Assuming that u_2 and u_4 vanish at $\rho = R_1, R_2$, we get

$$u_2 = \sum_{n=1}^{\infty} b_n^{(2)} \psi_n(k\rho) e^{j\nu_n(\theta-\alpha)} \tag{8}$$

$$u_4 = \sum_{n=1}^{\infty} b_n^{(4)} \psi_n(k\rho) e^{-j\nu_n(\theta+\alpha)} \tag{9}$$

with ${}^{\mathrm{s}}b_n^{(2)} = {}^{\mathrm{s}}b_n^{(4)}$ and ${}^{\mathrm{a}}b_n^{(2)} = -{}^{\mathrm{a}}b_n^{(4)}$. Lastly, u_5 is taken in the form

$$u_5 = \sum_{n=0(1)}^{\infty} \begin{Bmatrix} x_n^{\mathrm{s}} \cos n\theta' \\ x_n^{\mathrm{a}} \sin n\theta' \end{Bmatrix} \frac{H_n^{(2)}(k\rho')}{H_n^{(2)}(kr)} \tag{10}$$

where $x_n^{\mathrm{s}}, n = 0,1,...,$ and $x_n^{\mathrm{a}}, n = 1,2,...,$ are the expansion coefficients sought.

On the PEC surfaces, the boundary conditions can be written as

$$u_1 + u_3 + u_5 = 0,\ \rho = R_1, R_2 \tag{11}$$

$$\sum_{i=1}^{5} u_i = 0,\ \rho' = r \tag{12}$$

In the interval $R_1 < \rho < R_2$ the continuity conditions for the tangential electric and magnetic fields are

$$\sum_{i=1}^{5} u_i = \begin{cases} E_y^{(1)}, \theta = -\alpha \\ E_y^{(3)}, \theta = +\alpha \end{cases} \tag{13}$$

$$\frac{\partial}{\partial \theta}\left(u_2 + u_4 + u_5\right) = \begin{cases} \dfrac{\partial E_y^{(1)}}{\partial \theta}, \theta = -\alpha \\ \dfrac{\partial E_y^{(3)}}{\partial \theta}, \theta = +\alpha \end{cases} \tag{14}$$

On satisfying the conditions (11)-(14) and using the orthogonality of the functions φ_n, we find an infinite system of linear algebraic equations (SLAE)

$$\left(\mathbf{I} + \mathbf{A}\right)\mathbf{x} = \mathbf{t} \tag{15}$$

with the nuclear matrix operator $\mathbf{A}$ (details of the procedure of such algebraisation are given in [11]). Here $\mathbf{I}$ is an identity. The structure of $\mathbf{A}$, the right-hand vector $\mathbf{t}$, and the proof of correctness of the mathematical model obtained are given in Appendix C.

On truncating the systems (15) and subsequent inverting, the $\mathbf{x}^{\mathrm{s}}, \mathbf{x}^{\mathrm{a}}$ are found. Let $\mathbf{A}^{N,M} \overset{def}{=} \left\{a_{mn}^{N}\right\}_{m,n=1}^{M}$ be a truncation of the nuclear operator (N is a number of modes retained in the regions I, III) and $\mathbf{x}^{N,M}$ be the solution of a “truncated” counterpart of SLAE (15). Then the relative error of approximation

$$\delta\left(N,M\right) = \frac{\left\|\mathbf{x} - \mathbf{x}^{N,M}\right\|}{\left\|\mathbf{x}\right\|} \le \left\|\left(\mathbf{I} + \mathbf{A}\right)^{-1}\right\|\left\|\mathbf{A} - \mathbf{A}^{N,M}\right\| \tag{16}$$

tends to zero with $M,N \to \infty$ because the first factor in the right-hand part of inequality is a bounded constant, while the second one is decreasing [14]. The rate of decay of the function $\delta(N,M)$ can be taken as the cost of the algorithm [15]. As an alternative estimate of truncation errors the function

$$\Delta(K) = \frac{\left\| \mathbf{x}^K - \mathbf{x}^{K+1} \right\|}{\left\| \mathbf{x}^K \right\|}, K = N, M \tag{17}$$

can be used too [16]. The behaviours of the functions $\delta(N,M)$ and $\Delta(K)$ are illustrated in next section.

Scattering parameters, with $z = -0, +0$ as terminal planes, can be expressed through expansion coefficients as

$$\begin{aligned} S_{11} = S_{22} &= \left({}^sC_1^R + {}^aC_1^R \right) e^{j2v_1\alpha} \\ S_{12} = S_{21} &= \left({}^sC_1^T - {}^aC_1^T \right) e^{j2v_1\alpha} \end{aligned} \tag{18}$$

In a single-mode band, the normalised parameters of an equivalent T-circuit of the post junction can be found as in [6]

$$X_L = \frac{-j2S_{21}}{\left[(1-S_{11})^2 - S_{21}{}^2 \right]}; \quad X_C = j\frac{1+S_{11}-S_{21}}{1-S_{11}+S_{21}} \tag{19}$$

3. Numerical results

The algorithm proposed is a very efficient one in the numerical implementation. Table 1 illustrates convergence of the algorithm subject to geometrical parameters of the unit. The rate of stabilisation is extremely fast with respect to the truncation number M. It is also seen that the unitary property of the S-matrix holds with a high precision.

The error functions (16) and (17) are shown in Figs. 2a and 2b. In computing δ, the data corresponded to $M = 20, N = 60$ have been fixed as the reference values. One can see that it is enough to take few equations to achieve the accuracy, which is sufficient for engineering needs. As a result $N = 14$ and the 4×4 SLAE can be proposed for the evaluation of physical characteristics. For this size of the truncated matrix the accuracy is $\delta < 5\cdot10^{-4}$. Fig. 2b also shows typical values of the condition number, which are fairly close to the unity. In all the cases, we cite the greater values of the errors and condition numbers found in the numerical process for two subproblems considered.

According to known approximate approach, a strip is used to simulate the thin post in a straight guide [10]. The admissibility of this substitution for a curved guide was indicated in [12, 17]. Using Lewin's method for the first-order approximation [10], the relations

$$X_C \approx 0$$

$$X_L \approx \frac{\nu_1}{\psi_1(R_p)\psi_1(R_p + r)} \sum_{m=2}^{\infty} \frac{1}{2j\nu_m} \psi_m(R_p)\psi_m(R_p + r) \tag{20}$$

have been obtained [17]. The comparison with the latter as well as with the limiting case of a straight guide $(R_1 \to \infty, a = const)$ is given in Fig. 3. Here, the normalised reactances (19) are exhibited as a function of r/a for the centered post $(d = a)$, various curvatures and a fixed operation frequency. It is interesting to view that the thin-strip approximation (20) is more suitable for a large curvature than a small one. One can see that a slight deviation from the straight guide data takes place even for a sharp bend with $R_1 < a\,(R_1/R_2 < 1/3)$.

Fig. 4 presents the normalised reactances as a function of r/a for the off-centered post $(d = 0.6a)$ and various ratios R_1/R_2. In contrast to the previous case, the reactance X_C depends strongly on the curvature and the curves begin to disperse distinctly just for thin posts $(r \approx 0.05a)$. The effect is correlated with a noticeable shift of E_y-distribution from the post, as it is illustrated in Fig. 5. In Fig. 4, the X_L curve behaviour indicates that the range, within which the approximation (20) is valid, is sufficiently smaller.

Figs. 6 and 7 present the reactances depending on the position of the post centre, operating wavelength and the curvature. The asymmetry of the characteristics about the medial line of the waveguide is clearly visible. It is seen that there are positions of the post and frequency points where X_L or X_C is practically independent of the curvature.

The following figures are dealing with the current induced on the post surface. The current can be derived from the electric field as follows

$$\mathbf{J} = -\frac{1}{j\omega\mu_0}\left[\hat{\mathbf{u}}_{\rho'} \times \left(\nabla \times \mathbf{E}_y\right)\right]_{\rho'=r} = \frac{\hat{\mathbf{u}}_y}{j120\pi k}\sum_{i=1}^{5}\left\{\frac{\partial u_i}{\partial \rho'}\right\}_{\rho'=r} \tag{21}$$

where $\hat{\mathbf{u}}_{\rho'}$ and $\hat{\mathbf{u}}_y$ denote the unit vectors in the ρ' and y directions, respectively. Figs. 8 and 9 show the current distributions against azimuth θ' for the centered and off-centered posts respectively. Here, the intervals $\left(-180^\circ, 0\right)$ and $\left(0, 180^\circ\right)$ correspond to the “illuminated” portion of the post surface and the “shadow” one. Because of nonzero curvature the current has asymmetric distribution in both regions even for the centered-post structure. In the case of a smooth enough bend, the results are in good agreement with the data from [7, 11].

4. Conclusions

The problem of a circular inductive post in a uniformly curved rectangular waveguide has been solved using the DPT. All the cases of thin and large $(0 < r < a)$ arbitrarily placed $(R_1 < R_p < R_2)$ posts have been considered over a broad range of curvature variation $(0.1 \le R_1 / R_2 < 1)$. Taking advantage of the physical symmetry plane, the problem has been partitioned into two independent subproblems differing in a mode of excitations to get the maximum efficiency of the computational procedure.

The initial boundary value problem has been reduced to an infinite SLAE. It has been proved analytically that the matrix equation is of the Fredholm type with the nuclear operator. The rapidly convergent numerical algorithm has been developed to obtain the scattering matrix, the parameters of the equivalent T-network and the current induced on the post surface. The new data have been determined with low computational cost and at the same time the accuracies achieved are excellent with respect to any engineering needs.

The results computed show the good correlation with the approximate solution, which has been derived by the Lewin method. All the data obtained for a smooth bend $\left(R_1 / R_2 \geq 0.9\right)$ agree well with those for the limiting case of a straight guide.

Over full waveguide bandwidth, the paper provides one with the data that are essential in the design of devices containing the uniform bends with posts, such as transmission resonators or band-pass filters.

5. References

1. MARCUVITZ, N.: ‘Waveguide handbook’, IEE Electromagnetic Waves Series 21 (Peter Peregrinus, England, 1986)
2. ESTEBAN, H., COGOLLOS, S., BORIA, V. E., SAN BLAS, A., and FERRANDO, M.: ‘A new hybrid mode-matching/numerical method for the analysis of arbitrarily shaped inductive obstacles and discontinuities in rectangular waveguides’, *IEEE Trans. Microwave Theory Tech.*, 2002, **50**, (4), pp. 1219-1224
3. REITER, J. M., and ARNDT, F.: ‘Rigorous analysis of arbitrarily shaped H- and E-plane discontinuities in rectangular waveguides be a full-wave boundary contour mode-matching method’, *IEEE Trans. Microwave Theory Tech.*, 1995, **43**, (4), pp. 796-801
4. ABDULNOUR, J., and MARCHILDOR, L.: ‘Boundary elements and analytic expansions applied to H-plane waveguide junction’, *IEEE Trans. Microwave Theory Tech.*, 1994, **42**, (6), pp. 1038-1045
5. ISE, K., and KOSHIBA, M.: ‘Numerical analysis of H-plane waveguide junctions by combination of finite and boundary elements’, *IEEE Trans. Microwave Theory Tech.*, 1988, **36**, (9), pp. 1343-1351
6. LEVIATAN, Y., LI, P.G., ADAMS A.T., and PERINI, J.: ‘Single-post inductive obstacle in rectangular waveguide’, *IEEE Trans. Microwave Theory Tech.*, 1983, **31**, (10), pp. 806-811
7. LEVIATAN, Y., SHAU, D.H., and ADAMS A.T.: ‘Numerical study of the current distribution on a post in a rectangular waveguide’, *IEEE Trans. Microwave Theory Tech.*, 1984, **32**, (10), pp. 1411-1415
8. SCHWINGER, J., and SAXON, D.S.: ‘Discontinuities in waveguides’ (Gordon and Broach, New York, 1968)
9. NIELSEN, E.D.: ‘Scattering by a cylindrical post of complex permittivity in a waveguide’, *IEEE Trans. Microwave Theory Tech.*, 1967, **17**, (3), pp.148-153

10. LEWIN, L.: ‘Theory of waveguides’ (Neurnes Butterworths, London, 1975)

11. CHUMACHENKO, V.P., and PETRUSENKO, I.V.: ’Domain product solution for scattering by cylindrical obstacle in rectangular waveguide’, *Electromagnetics*, 2002, 22, (6), pp.473-486

12. VOL’MAN, V.I., and KNIZHNIK, A.I.: ’Analysis of inductive post in continuously curved waveguide,’ *Radiotehnika*, 1980, 35, (8), pp. 72-75 (in Russian)

13. CHUMACHENKO, V.P.: ‘The use of the integral equation method for solving one class of electrodynamics problems,’ *Izvestiya VUZ. Radiofizika*, 1978, **21**, (7), pp. 1004-1010 (in Russian)

14. REED, M, and SIMON, B.: ‘Methods of modern mathematical physics. v.1. Functional analysis’ (Academic Press, New York, 1978)

15. NOSICH, A.I.: ‘The method of analytical regularisation in wave-scattering and eigenvalue problems: foundations and review of solutions,’ IEEE Antennas and Propag. Magazine, 1999, **41**, (3), pp. 34-49

16. NOSICH, A.I., OKUNO, Y., and SHIRAISHI, T.: ‘Scattering and absorption of E- and H-polarised plane waves by a circularly curved resistive strip,’ *Radio Science*, 1996, **31**, (6), pp. 1733-1742

17. PETRUSENKO, I.V., KODAK, S.N., and ESSERT, V.E.: ‘Single-post inductive obstacle in continuously curved waveguide.’ Bulletin “Calculation and measurement of parameters of microwave components”, Dnipropetrovs’k State University, 1988, p.62-66 (in Russian)

18. MORSE, P.M., and FESHBACH, F.: ‘Methods of theoretical physics’ (McGraw-Hill, New York, Toronto, London, 1953)

19. WATSON, G.N.: ‘A treatise on Bessel functions’ (Cambridge University Press, 1944) 2nd edn.

20. PETRUSENKO, I.V.: ‘Higher-order approximation of wave propagation constants in the uniformly curved waveguide.’ *IEE Proc.-Microw. Antennas Propag*., 2001, 148, (5), pp.280-284

Appendix A

In a cylindrical frame, Fig. 1, the solution of the Helmholtz equation can be easily found via the variable separation method. Considering $LM_{m0}, m = 1, 2, ...,$ modes as circulating waves, an appropriate form for their E_y -component is

$$E_y = \upsilon_\nu (k\rho) e^{\pm j\nu\theta} \tag{22}$$

Here $\upsilon_\nu (k\rho)$ is an eigenfunction of the Sturm-Liouville problem for Bessel's equation of order ν. On the finite interval $0 < R_1 \le \rho \le R_2$, the set of these eigenfunctions forms a complete orthonormal set of square integrable functions [18].

On the two curved walls E_y must vanish, and this leads to the cross-product Bessel function

$$\upsilon_\nu (k\rho) = c\left[J_\nu (k\rho) N_\nu (kR_2) - J_\nu (kR_2) N_\nu (k\rho) \right] \equiv cP_\nu (k\rho, kR_2) \tag{23}$$

and to the modal equation

$$P_{\nu_m} (kR_1, kR_2) = 0 \tag{24}$$

In eqn. (23), the norming quantity c is found according to the relationship between solutions of the Bessel equation [19]

$$\int \upsilon_\nu (k\rho) u_\mu (k\rho) \frac{d\rho}{\rho} = \frac{\rho}{\nu^2 - \mu^2} \left[\frac{\partial \upsilon_\nu}{\partial \rho} u_\mu - \upsilon_\nu \frac{\partial u_\mu}{\partial \rho} \right] \tag{25}$$

from which it follows

$$\int_{R_1}^{R_2} P_\nu (k\rho, kR_2)\, P_\mu (k\rho, kR_2) \frac{d\rho}{\rho} = \delta_{\nu\mu} \left[\frac{\rho}{2\nu} \frac{\partial P_\nu (k\rho, kR_2)}{\partial \rho} \frac{\partial P_\nu (k\rho, kR_2)}{\partial \nu} \right]_{\rho = R_1} \tag{26}$$

Here $\delta_{\nu\mu}$ is the Kronecker delta.

In this paper, we use the special norm

$$\left\|P_{\nu}\right\| = \left[\frac{\rho}{\sigma\nu} \frac{\partial P_{\nu}\left(k\rho, kR_2\right)}{\partial\rho} \frac{\partial P_{\nu}\left(k\rho, kR_2\right)}{\partial\nu} \right]_{\rho=R_1}^{1/2}, \sigma = \ln\left(\frac{R_2}{R_1}\right) \tag{27}$$

according to the orthogonality condition for the cross eigenfunctions (3)

$$\int_{R_1}^{R_2} \psi_m\left(k\rho\right)\psi_n\left(k\rho\right)\frac{d\rho}{\rho} = \frac{\sigma}{2}\delta_{mn} \tag{28}$$

It provides the required quasistatic approximation for $m >> 1$

$$\psi_m\left(k\rho\right) \simeq \sin\left[\frac{m\pi}{\sigma}\ln\left(\frac{R_2}{\rho}\right)\right] \tag{29}$$

The high-order approximation to the angular propagation constant ν_m, $m = 1, 2, \ldots$, and $k-\nu$ diagram for the modal equation (24) are given in [20].

Appendix B

In order to avoid division by zero during computations let us construct the solution of the Bessel equation

$$\hat{W}_n\left(k\rho\right) = AJ_{\mu_n}\left(k\rho\right) + BN_{\mu_n}\left(k\rho\right), \qquad \tilde{R} \le \rho \le R_2 \tag{30}$$

which does not vanish for any real value of the wavenumber. For this purpose $\hat{W}_n$ must satisfy

- boundary condition of the impedance type $\hat{W}_n\left(k\tilde{R}\right) + j\tilde{R}\dfrac{\partial\hat{W}_n\left(k\tilde{R}\right)}{\partial\tilde{R}} = 0$;

- normalisation condition $\hat{W}_n\left(kR_2\right)=1$;

- additional requirement $\lim_{n\to\infty}\hat{W}_n\left(k\rho\right)=0,\ \tilde{R}<\rho<R_2$ for robust calculations.

The solution sought takes the form

$$\hat{W}_n\left(k\rho\right)=\frac{W_{\mu_n}\left(k\rho\right)}{W_{\mu_n}\left(kR_2\right)} \tag{31}$$

$$W_\mu\left(k\rho\right)=P_\mu\left(k\tilde{R},k\rho\right)+j\tilde{R}\frac{\partial P_\mu\left(k\tilde{R},k\rho\right)}{\partial\tilde{R}} \tag{32}$$

Appendix C

Below the designations

$$p=\begin{Bmatrix}2m\\2m-1\end{Bmatrix},\ q=\begin{Bmatrix}2n\\2n-1\end{Bmatrix},\ cs_n\left(\theta\right)=\begin{Bmatrix}\cos n\theta\\\sin n\theta\end{Bmatrix},\ fe_n\left(\theta\right)=2e^{-i\nu_n\alpha}\begin{Bmatrix}\cos\nu_n\theta\\i\sin\nu_n\theta\end{Bmatrix} \tag{33}$$

are used to make formulae less cumbersome. Hereinafter, the upper and lower symbols are connected with the symmetric and antisymmetric case respectively.

It can be shown in analogy to the result of the paper [11] that in eqn. (15) the matrix operator has the structure

$$\mathbf{A}=(\mathbf{T}_1\mp\frac{1}{2}\hat{\mathbf{T}}_2\mathbf{F}_1)\mathbf{D}_1+(\mathbf{T}_3\mp\frac{1}{2}\hat{\mathbf{T}}_2\mathbf{F}_3)\mathbf{D}_3\mp\frac{1}{2}\hat{\mathbf{T}}_2\left(\mathbf{F}_2-\mathbf{G}\right) \tag{34}$$

Let us introduce an auxiliary vector

$$\boldsymbol{\tau}^{(n)}\left(\rho,\theta\right)=\left(\hat{H}_q\left(k\rho\right)\varphi_q\left(\theta\right);\psi_n\left(k\rho\right)fe_n\left(\theta\right);\hat{W}_q\left(k\rho\right)\varphi_q\left(\theta\right)\right) \tag{35}$$

then the elements of $\mathbf{T}_i,\ i=1,2,3,$ and $\hat{\mathbf{T}}_2$ can be expressed in the form

$$t_{mn}^{(i)} = \frac{2}{\varepsilon_m \pi} \int_0^{\pi} \left[\tau_i^{(n)} (\rho, \theta) \right]_{\rho'=r} cs_m (\theta') d\theta' ; \quad \hat{t}_{mn}^{(2)} = n^{1/2} t_{mn}^{(2)} ; \quad \varepsilon_m = \begin{cases} 2, m = 0 \\ 1, m \geq 1 \end{cases} \tag{36}$$

The elements of $\mathbf{F}_i, i = 1, 2, 3,$ and $\mathbf{G}$ are described by the formulae

$$f_{mn}^{(1)} = \frac{2m^{-1/2}}{\sigma (\mu_q^2 - \nu_m^2)} \left\{ \frac{2}{\pi} \hat{H}_q (kR_2) \left\| P_{\nu_m} \right\|^{-1} + \left[\rho \frac{\partial \psi_m (k\rho)}{\partial \rho} \right]_{\rho = R_1} \right\} \tag{37}$$

$$f_{mn}^{(2)} = \frac{2}{\sigma m^{1/2}} \int_{R_1}^{R_2} \left[cs_n (\theta') \frac{H_n^{(2)} (k\rho')}{H_n^{(2)} (kr)} \right]_{\theta = -\alpha} \psi_m (k\rho) \frac{d\rho}{\rho} \tag{38}$$

$$f_{mn}^{(3)} = \frac{2m^{-1/2}}{\sigma (\mu_q^2 - \nu_m^2)} \left\{ \frac{2}{\pi} \left\| P_{\nu_m} \right\|^{-1} + \left[\rho \frac{\partial \psi_m (k\rho)}{\partial \rho} \right]_{\rho = R_1} \hat{W}_q (kR_1) \right\} \tag{39}$$

$$g_{mn} = \frac{2m^{-1/2}}{j\sigma \nu_m} \int_{R_1}^{R_2} \left\{ \frac{\partial}{\partial \theta} \left[cs_n (\theta') \frac{H_n^{(2)} (k\rho')}{H_n^{(2)} (kr)} \right] \right\}_{\theta = -\alpha} \psi_m (k\rho) \frac{d\rho}{\rho} \tag{40}$$

Matrices $\mathbf{D}_i, i = 1, 3,$ are defined by the elements

$$d_{mn}^{(1)} = \Lambda_p^{-1} \left[d_{mn}^{-} - \hat{W}_p (kR_1) d_{mn}^{+} \right], \quad d_{mn}^{(3)} = \Lambda_p^{-1} \left[d_{mn}^{+} - \hat{H}_p (kR_2) d_{mn}^{-} \right] \tag{41}$$

where

$$\Lambda_p = 1 - \hat{H}_p (kR_2) \hat{W}_p (kR_1) \tag{42}$$

$$d_{mn}^{+,-} = -\frac{2}{\varepsilon_p \alpha} \int_0^{\alpha} \left[cs_n (\theta') \frac{H_n^{(2)} (k\rho')}{H_n^{(2)} (kr)} \right]_{\rho = R_2, R_1} \varphi_p (\theta) d\theta, \tag{43}$$

Finally, the right-hand part of eqn. (15) takes the form $\mathbf{t} \equiv \left\{ \mp t_{m1}^{(2)} / 2 \right\}$.

The proof of the correctness of the proposed model is based on the Fredholm property of eqn. (15). It is sufficient to show that $\mathbf{A}$ is a compact matrix operator in the Hilbert space

$$h_1 \overset{def}{=} \left\{ x_n : \sum_{n=0}^{\infty} (n+1) |x_n|^2 < \infty \right\} \tag{44}$$

and the right-hand part $\mathbf{t} \in h_1$ [14].

Compactness of the operator (34) follows from asymptotic estimates of the integrals (36), (38), (40) and (43), which are Fourier's coefficients of the functions being differentiable infinitely many times. Namely, the estimation formulae

$$\left|t_{mn}^{(1,3)}\right| = O\left[\frac{e^{-\mu_q l_{1,3}}}{m!}\left(\mu_q \frac{r}{R_p}\right)^m\right], \left|\hat{t}_{mn}^{(2)}\right| = O\left[\frac{e^{-n\pi l_2}}{m!} n^{m+1/2}\left(\frac{\pi r}{\sigma R_p}\right)^m\right]; m,n \gg 1; r \ll R_p \qquad (45)$$

$$\mathbf{l} = \left(\ln\left(\frac{R_p}{R_1}\right), \frac{\alpha}{\sigma}, \ln\left(\frac{R_2}{R_p}\right)\right)$$

give us $\mathbf{t} \in h_1$ and lead to the inequalities

$$\begin{aligned} &\sum_{m,n}^{\infty} m\left|t_{mn}^{(1,3)}\right|^2 = O\left[\left(1-\zeta_{1,3}\right)^{-\beta}\right] < \infty \\ &\sum_{m,n}^{\infty} m\left|\hat{t}_{mn}^{(2)}\right|^2 = O\left[\left(1-\zeta_2\right)^{-\tau}\right] < \infty \\ &\boldsymbol{\zeta} = \left(\frac{r}{d}, \frac{r}{\alpha R_p}, \frac{r}{2a-d}\right), \beta > \tau > 0 \end{aligned} \qquad (46)$$

under conditions $\zeta_i < 1, i = 1,2,3$. Hence, $\mathbf{T}_{1,3}, \hat{\mathbf{T}}_2$ are the Hilbert-Schmidt (H.-S.) operators $h_1 \to h_1$ [14] provided that the post does not touch the boundaries of the interaction region II. Under the same condition, we get

$$\begin{aligned} &\sum_{m,n}^{\infty}\left|f_{mn}^{(1,3)}\right|^2 < \infty, \sum_{m,n}^{\infty}\frac{1}{n}\left|\xi_i^{(m,n)}\right|^2 < \infty, i = 1,2,3 \\ &\boldsymbol{\xi}^{(m,n)} = \left(f_{mn}^{(2)}, g_{mn}, d_{mn}^{(1,3)}\right) \end{aligned} \qquad (47)$$

Therefore, $\mathbf{D}_1, \mathbf{D}_3, \mathbf{G}, \mathbf{F}_i,\ i = 1,2,3,$ present the H.-S. operators as well. Thus, $\mathbf{A}: h_1 \to h_1$ is the nuclear operator as a sum of products of the H.-S. operators [14].

Table 1. Scattering characteristics subject to the truncation numbers M, N and the parameters d, r and R_1/R_2 for $\lambda/2a = 1.4286$, $\left(PCL = |S_{11}|^2 + |S_{21}|^2, ORT = S_{11}\overline{S}_{21} + S_{12}\overline{S}_{22}\right)$.

$d/a = 0.2, r/a = 0.1, N = 40$					
R_1/R_2	M	$\|S_{11}\|$	$\arg S_{11}$	PCL	ORT
0.1	1	0.088746	1.705305	1.000003	0.000004
	2	0.088546	1.706329	1.000003	0.000004
	4	0.088536	1.706341	1.000003	0.000004
	8	0.088536	1.706341	1.000003	0.000004
	12	0.088536	1.706341	1.000003	0.000004
0.4	1	0.139468	1.730135	0.999999	-0.000001
	2	0.138933	1.730920	0.999999	-0.000001
	4	0.138932	1.730921	0.999999	-0.000001
	8	0.138932	1.730921	0.999999	-0.000001
	12	0.138932	1.730921	0.999999	-0.000001
0.9	1	0.151754	1.733333	1.000002	0.000002
	2	0.151394	1.733933	1.000001	0.000001
	4	0.151406	1.733935	1.000001	0.000001
	8	0.151406	1.733935	1.000001	0.000001
	12	0.151406	1.733935	1.000001	0.000001
$d/a = 0.2, r/a = 0.1, M = 10$					
R_1/R_2	N	$\|S_{11}\|$	$\arg S_{11}$	PCL	ORT
0.1	2	0.096980	1.531685	1.026847	0.029461
	5	0.087857	1.695090	1.001607	0.001853
	10	0.088511	1.705070	1.000170	0.000223
	20	0.088533	1.706186	1.000025	0.000031
	40	0.088536	1.706341	1.000003	0.000004
0.4	2	0.135502	1.728173	1.001399	-0.000119
	5	0.138662	1.733175	0.999324	-0.000705
	10	0.138918	1.731010	0.999976	-0.000030
	20	0.138930	1.730933	0.999996	-0.000005
	40	0.138932	1.730921	1.000000	-0.000001
0.9	2	0.148575	1.715790	1.004367	0.004387
	5	0.151204	1.734106	0.999877	-0.000121
	10	0.151390	1.733814	1.000034	0.000034
	20	0.151396	1.733921	1.000005	0.000005
	40	0.151396	1.733935	1.000001	0.000001
$d/a = 1, r/a = 0.5, N = 40$					
R_1/R_2	M	$\|S_{11}\|$	$\arg S_{11}$	PCL	ORT
0.1	1	0.999999	-1.994400	0.999998	0.000001
	2	0.999770	-1.918815	0.999999	0.000001
	4	0.999889	-1.911811	0.999999	0.000001
	8	0.999889	-1.911795	0.999999	0.000001
	12	0.999889	-1.911795	0.999999	0.000001
0.9	1	0.997720	-1.924362	0.999999	0.000000
	2	0.999985	-1.851008	0.999999	0.000000
	4	0.999999	-1.844055	0.999999	0.000000
	8	0.999999	-1.844053	0.999999	0.000000
	12	0.999999	-1.844053	0.999999	0.000000
$d/a = 1, r/a = 0.5, M = 10$					
R_1/R_2	N	$\|S_{11}\|$	$\arg S_{11}$	PCL	ORT
0.1	2	0.986429	-1.912672	0.973209	0.024541
	5	0.999654	-1.911519	0.999518	0.000377
	10	0.999844	-1.911772	0.999907	0.000079
	20	0.999884	-1.911792	0.999988	0.000010
	40	0.999889	-1.911795	0.999999	0.000001
0.9	2	0.992587	-1.847440	0.985337	0.005329
	5	0.999732	-1.843906	0.999464	-0.000156
	10	0.999963	-1.844051	0.999927	0.000008
	20	0.999995	-1.844052	0.999990	0.000000
	40	0.999999	-1.844053	0.999999	0.000000

FIGURE CAPTIONS

Fig. 1. Geometry of the problem and pertinent co-ordinate systems.

Fig. 2. The error functions δ and Δ against (a) the number of modes N in the curved waveguide and (b) the matrix truncation number M (left-hand logarithmic axes). (b) Condition number of the matrix approximation (right-hand linear axis). $r = 0.25a, d = a, \lambda / 2a = 1.4$, $R_1 / R_2 = 0.5$.

Fig. 3. Circuit parameters against a radius size for centered post, $\lambda / 2a = 1.4$.

Fig. 4. Circuit parameters against a radius size for off-centered post, $d = 0.6a$, $\lambda / 2a = 1.4$.

Fig. 5. The transverse distribution of the E_y-component of the incident wave and the relative position of the off-centered posts of various sizes, $\lambda / 2a = 1.4$.

Fig. 6. Circuit parameters against position of the post for $r = 0.3a, \lambda / 2a = 1.2$.

Fig. 7. Circuit parameters against $\lambda / 2a$ for off-centered large post, $d = 0.6a, r = 0.3a$.

Fig. 8. Real part (a) and imaginary part (b) of the surface current on the centered post, $\lambda / 2a = 1.2$.

Fig. 9. Real part (a) and imaginary part (b) of the surface current on the off-centered post, $d = 0.6a$, $\lambda / 2a = 1.2$.

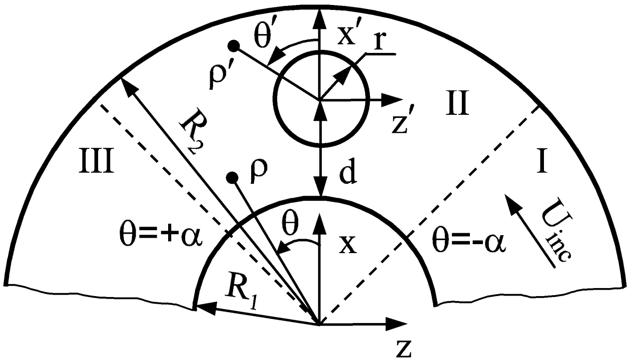

Fig. 1

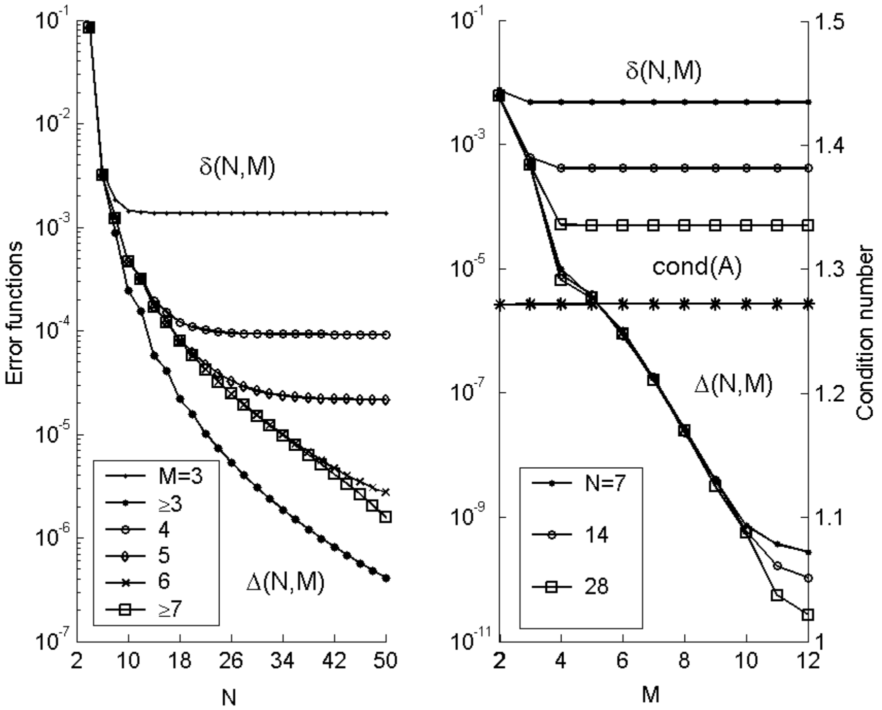

Error functions
δ(N,M)
Δ(N,M)
M=3
≥3
4
5
6
≥7
N
δ(N,M)
cond(A)
Δ(N,M)
N=7
14
28
M
Condition number

(a) (b)

Fig. 2

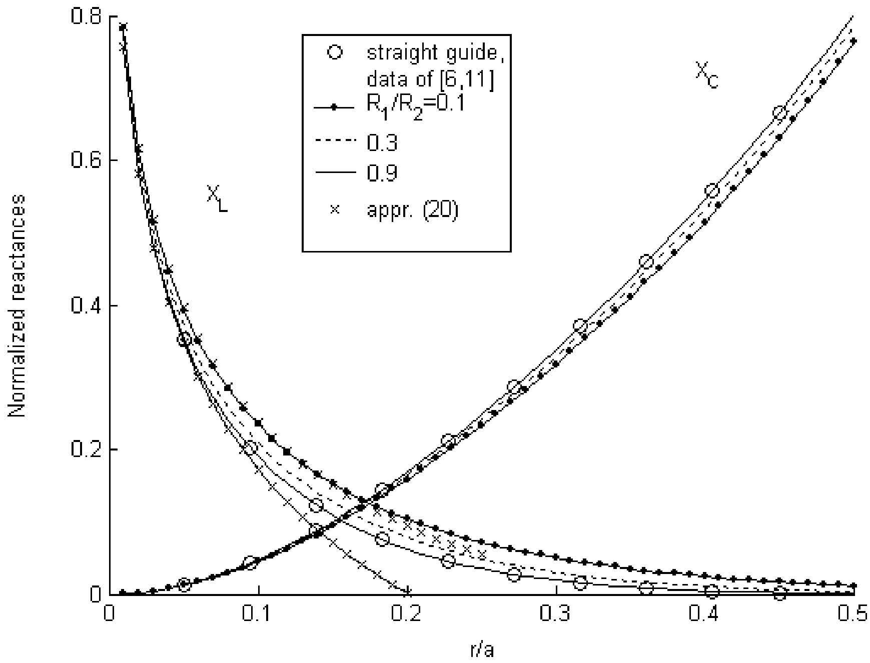

straight guide, data of [6,11]
R1/R2=0.1
0.3
0.9
appr. (20)
XL
XC
Normalized reactances
r/a
0.8
0.6
0.4
0.2
0
0.1
0.2
0.3
0.4
0.5

Fig. 3

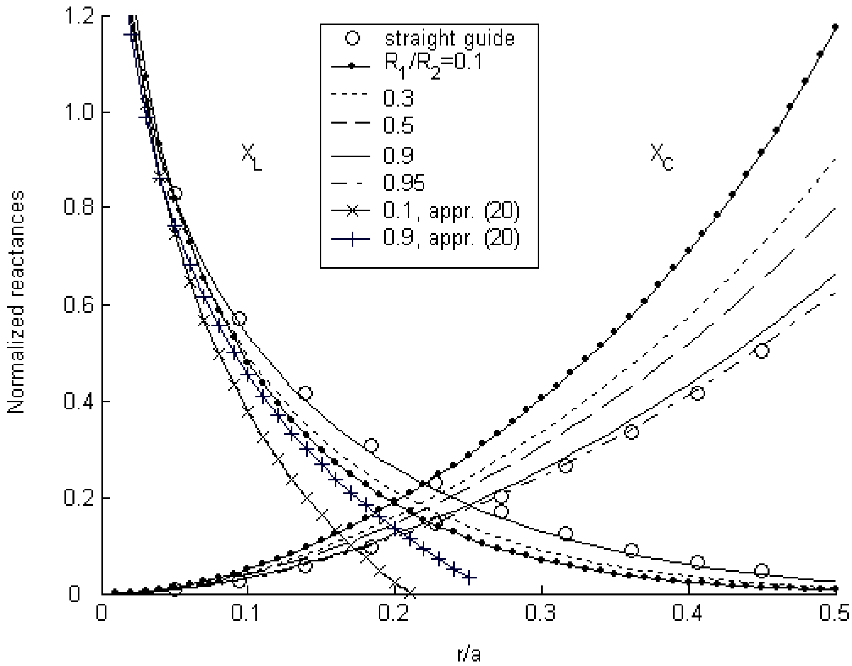

straight guide
R_1/R_2=0.1
0.3
0.5
0.9
0.95
0.1, appr. (20)
0.9, appr. (20)
X_L
X_C
Normalized reactances
r/a

Fig.4

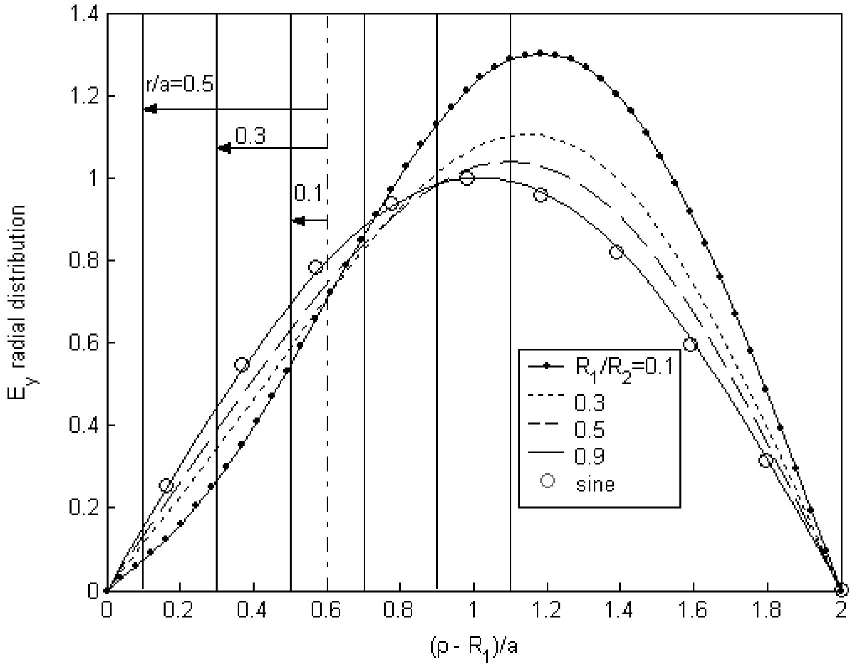

r/a=0.5
0.3
0.1
R_1/R_2=0.1
0.3
0.5
0.9
sine
E_y radial distribution
$(\rho - R_1)/a$
0
0.2
0.4
0.6
0.8
1
1.2
1.4
1.6
1.8
2

Fig. 5

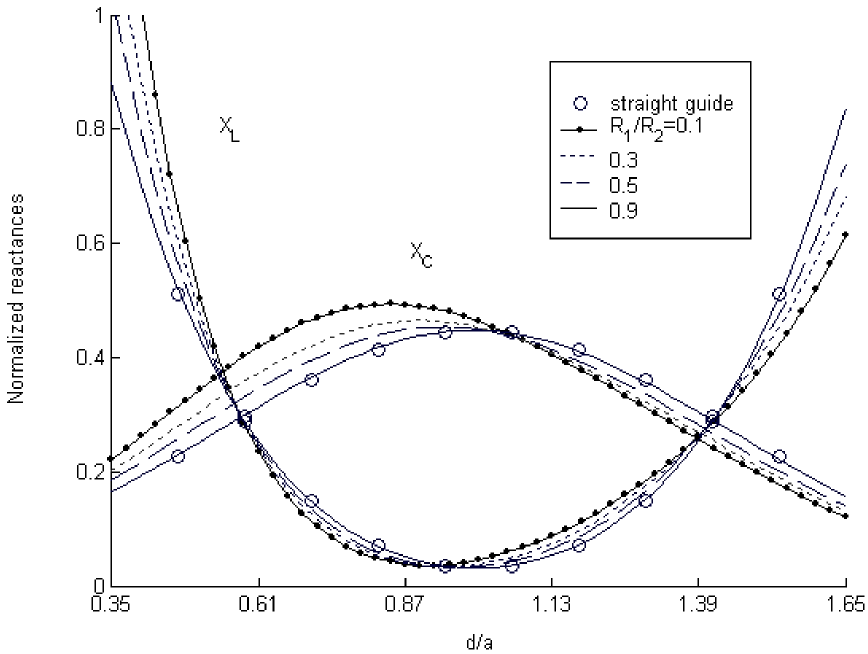

straight guide
R_1/R_2=0.1
0.3
0.5
0.9
X_L
X_C
Normalized reactances
d/a
0
0.2
0.4
0.6
0.8
1
0.35
0.61
0.87
1.13
1.39
1.65

Fig. 6

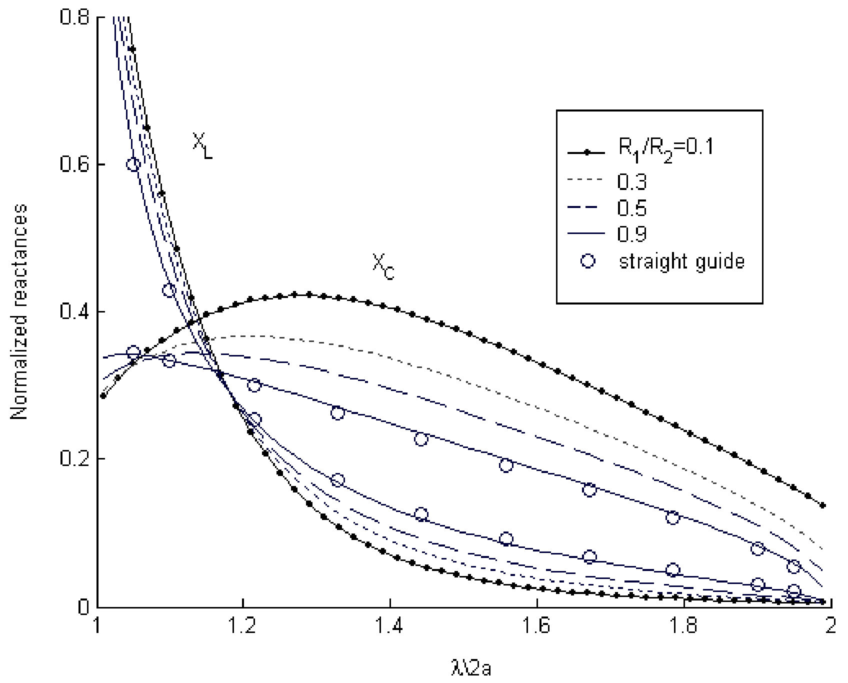
0.8
0.6
0.4
0.2
0
1
1.2
1.4
1.6
1.8
2
Normalized reactances
λ\2a
X_L
X_C
R_1/R_2=0.1
0.3
0.5
0.9
straight guide

Fig. 7

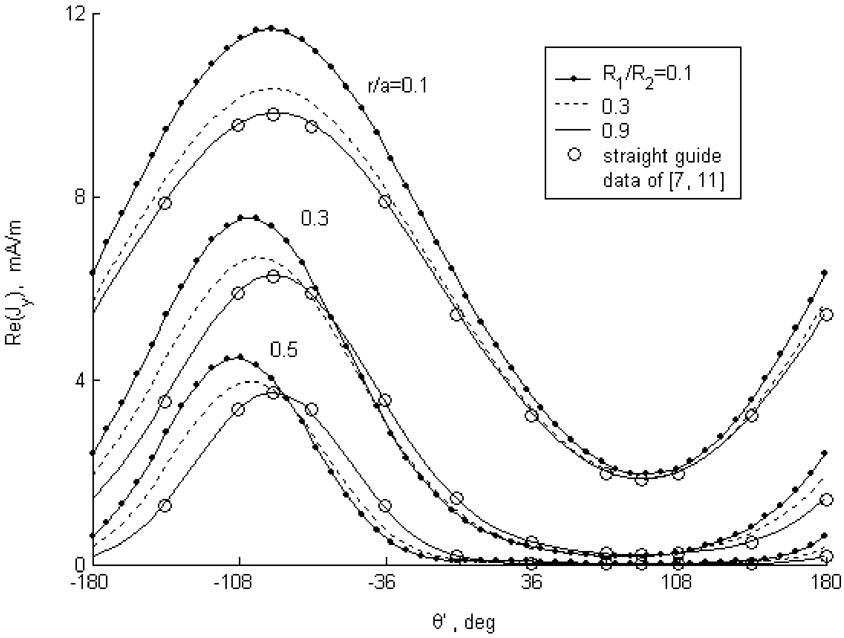

12
8
4
0
-180
-108
-36
36
108
180
Re(J_y), mA/m
θ', deg
r/a=0.1
0.3
0.5
R_1/R_2=0.1
0.3
0.9
straight guide
data of [7, 11]

Fig. 8a

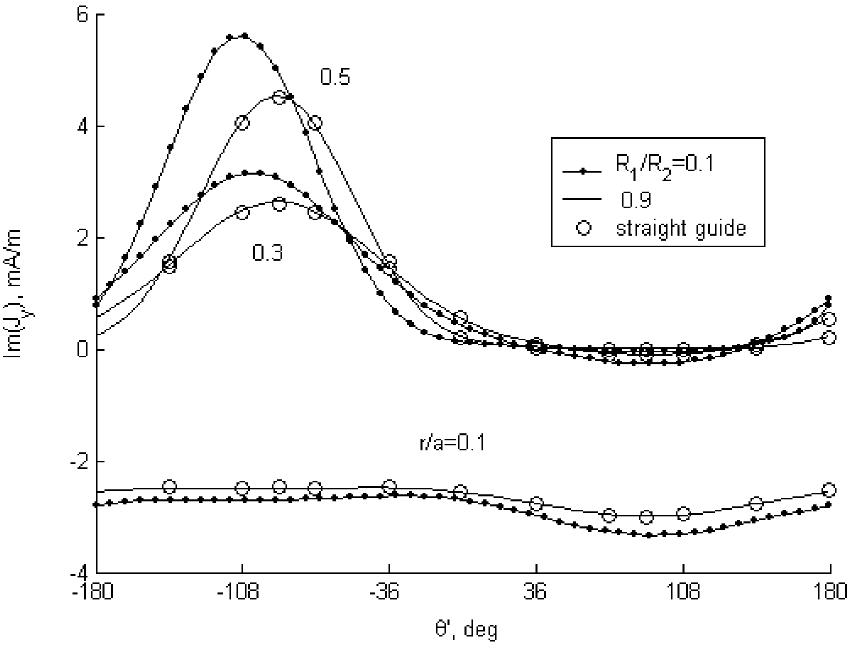

6
4
2
0
-2
-4
-180
-108
-36
36
108
180
Im(J_y), mA/m
θ', deg
0.5
0.3
r/a=0.1
R1/R2=0.1
0.9
straight guide

Fig. 8b

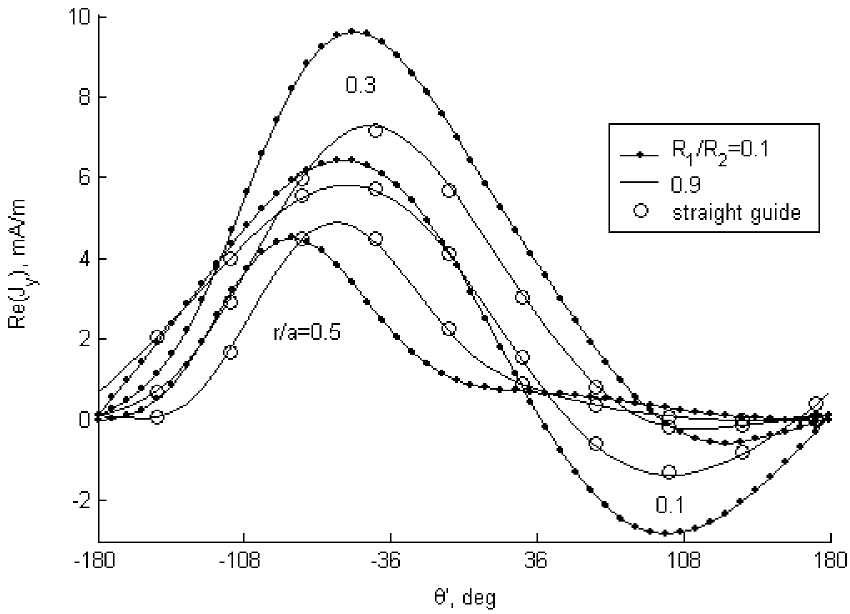

10
8
6
4
2
0
-2
Re(J_y), mA/m
0.3
R_1/R_2=0.1
0.9
straight guide
r/a=0.5
0.1
-180
-108
-36
36
108
180
θ', deg

Fig. 9a

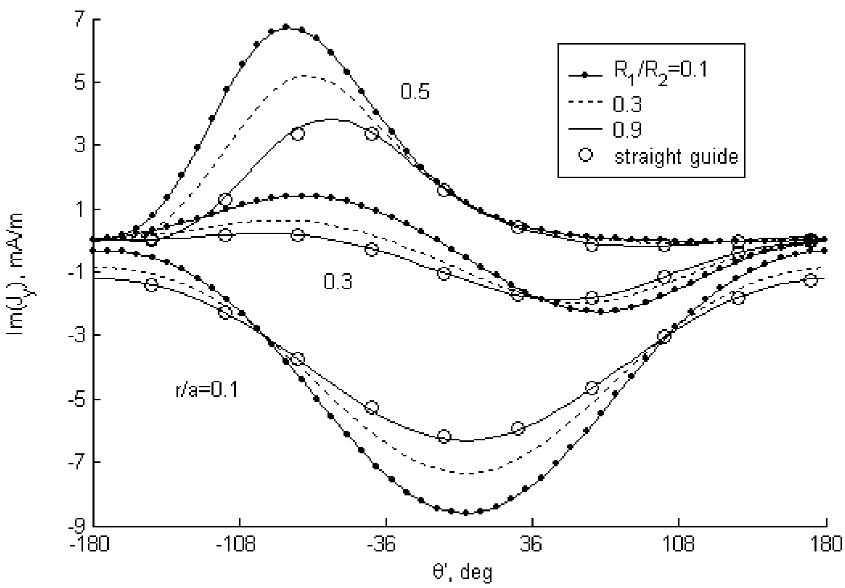

7
5
3
1
-1
-3
-5
-7
-9
-180
-108
-36
36
108
180
θ', deg
Im(J_y), mA/m
R1/R2=0.1
0.3
0.9
straight guide
0.5
0.3
r/a=0.1

Fig. 9b